Magnetic fields in galaxy clusters

Christoph Pfrommer[1]

in collaboration with

Jonathan Dursi[1,2]

[1] Canadian Institute for Theoretical Astrophysics, Canada
[2] SciNet Consortium, University of Toronto, Canada

May 20, 2010 / Institute for Advanced Study

CITA–ICAT

Outline

1. Magnetic draping
   - Space physics and clusters
   - Analytical calculations
   - MHD Simulations
2. Spiral galaxies
   - Polarized radio ridges
   - Physics of magnetic draping
   - Draping and synchrotron emission
3. Implications
   - Magnetic field orientations
   - Kinetic plasma instabilities
   - Cosmological evolution of galaxy clusters

CITA–ICAT

Outline

1. Magnetic draping
   - Space physics and clusters
   - Analytical calculations
   - MHD Simulations
2. Spiral galaxies
   - Polarized radio ridges
   - Physics of magnetic draping
   - Draping and synchrotron emission
3. Implications
   - Magnetic field orientations
   - Kinetic plasma instabilities
   - Cosmological evolution of galaxy clusters

CITA–ICAT

Draping field lines around a moving object

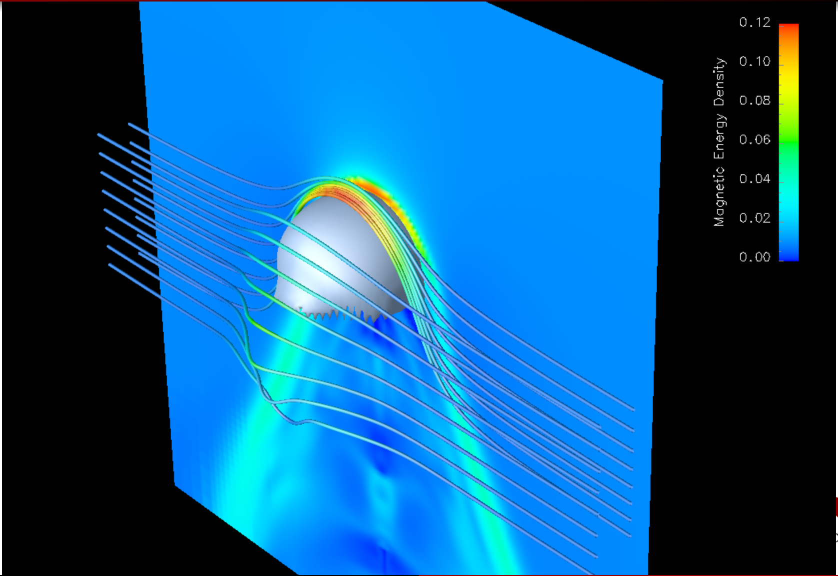

Draping of solar wind field around the Earth

- the Earth's dipolar field shields the surface from penetrating cosmic rays
- the magnetic dipole has reversed sign some hundreds of times over the last 400 million years, which corresponds to breakdowns of the dynamo action

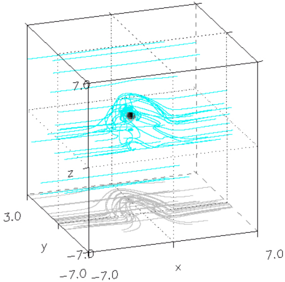

Birk, Lesch & Konz (2004)

- 3D plasma-neutral gas simulations show that the solar wind can induce very fast ($\sim$10 min) a strong magnetic field in the previously completely unmagnetized Earth's ionosphere
- Earth magnetic polarity reversals may not be catastrophic to life!

CITA–ICAT

Draping of Saturn's field over Titan's atmosphere

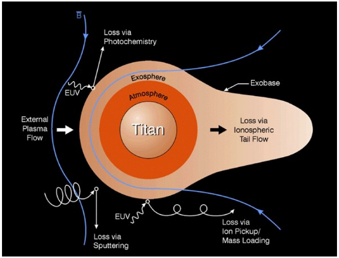

S. Ledvina, UC Berkeley

- draping of Saturn's magnetic field around Titan's ionosphere observed with Cassini: sharp draping boundary in near-tail region (Neubauer et al. 2006)
- emission from draping region and removal of neutrals and ions from Titan and added to Saturn's magnetosphere

Puzzles in galaxy clusters

- radio bubbles, seen as X-ray cavities, are observed out to large distances and have very sharp interfaces: hydrodynamic instabilities should disrupt them
- high-resolution X-ray data reveal 'cold fronts' with sharp edges in temperature and density: they are not expected to remain sharp in the presence of diffusion and thermal conduction for $\gtrsim 10^8$ yrs

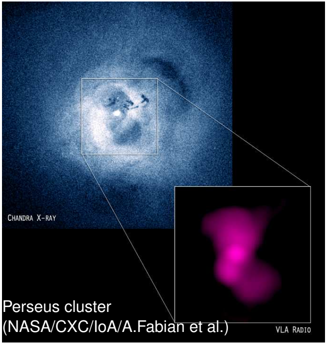

Perseus cluster (NASA/CXC/IoA/A.Fabian et al.)

→ Could bubble/core motions sweep up enough magnetic field to suppress instabilities and diffusion/conduction across the interface?

Idea: magnetic draping comes to rescue (Lyutikov 2004)

- analytics, B-profile along the stagnation line:

$$\frac{B}{\rho} = \frac{1}{\sqrt{1-\frac{R^3}{r^3}}}\,\frac{B_0}{\rho_0}, \qquad l_{\mathrm{drape}} \approx \frac{1}{\mathcal{M}_{\mathrm{A}}^2} R$$

- formula predicts infinite B-amplification at the contact that is in conflict with the kinematic assumption of negligible back-reaction

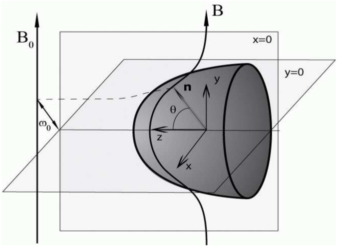

Lyutikov (2004)

→ need MHD simulations to account for the non-linear feedback!

CITA–ICAT

Magnetic draping at work in clusters

- rising radio bubbles in a hot atmosphere
- shown is the log of the density for the non-draping versus draping case (time increasing upwards)

  → draping suppresses hydrodynamical instabilities in accordance with observations

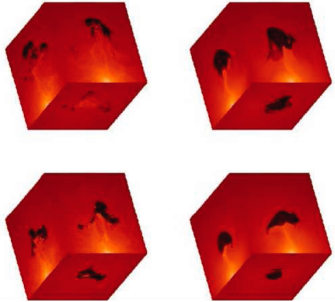

Ruszkowski et al. (2007)

CITA–ICAT

Potential flow around a moving sphere – 1

- origin $\mathcal{O}$ at the center of the sphere, constant inflow velocity $\boldsymbol{u}$
- incompressible ($\rho = \text{const}$): $\dot{\rho} + \text{div}\rho\boldsymbol{v} = 0 \quad \rightarrow \quad \text{div}\boldsymbol{v} = 0$
  $\boldsymbol{v} = \nabla\phi \quad \rightarrow \quad \Delta\phi = 0$
- boundary conditions: $\boldsymbol{v}\big|_\infty = \boldsymbol{0}$
- only solutions to $\Delta\phi = 0$ that vanish at infinity are $1/r$ and derivatives thereof with respect to the coordinates
- symmetry of the sphere $\rightarrow$ one constant vector in solution: $\boldsymbol{u}$
- linearity of $\Delta\phi = 0$ and boundary conditions $\rightarrow$ $\boldsymbol{u}$ can only enter linearly into ϕ: the only scalar that can be constructed is $\boldsymbol{u} \cdot \nabla\left(\frac{1}{r}\right)$
- ansatz: $\phi_\text{s} = \boldsymbol{A} \cdot \nabla\left(\frac{1}{r}\right) = -\frac{1}{r^2}\boldsymbol{A}\boldsymbol{e}_r$

CITA–ICAT

Potential flow around a moving sphere – 2

- ansatz: $\phi_{\mathrm{s}} = \boldsymbol{A} \cdot \nabla \left(\frac{1}{r}\right) = -\frac{1}{r^2}\, \boldsymbol{A}\boldsymbol{e}_r$
- the surface of the body does not allow flow through it; determine $\boldsymbol{A}$ from boundary condition $(\boldsymbol{v} - \boldsymbol{u})\boldsymbol{e}_r\big|_{r=R} \overset{!}{=} 0$:
  $$\boldsymbol{v}\boldsymbol{e}_r\big|_{r=R} = \boldsymbol{e}_r^2 \partial_r \phi_{\mathrm{s}}\big|_{r=R} = \frac{2}{r^3} \boldsymbol{A}\boldsymbol{e}_r\big|_{r=R} \overset{!}{=} \boldsymbol{u}\boldsymbol{e}_r \quad \rightarrow \quad \boldsymbol{A} = \frac{1}{2}\, R^3 \boldsymbol{u}$$
- potential in sphere-centered coordinate system: $\phi_{\mathrm{s}} = \frac{R^3}{2r^2}\, \boldsymbol{u}\boldsymbol{e}_r$
- transforming to lab system: $\phi_{\mathrm{trans}} = -uz = -ur\cos\theta = -r\boldsymbol{u}\boldsymbol{e}_r$
- potential $\phi = \phi_{\mathrm{s}} + \phi_{\mathrm{trans}} = -\left(\frac{R^3}{2r^2} + r\right)\, \boldsymbol{u}\boldsymbol{e}_r$
- $\boldsymbol{v} = \nabla\phi = \boldsymbol{e}_r \partial_r \phi + \boldsymbol{e}_\theta \frac{1}{r} \partial_\theta \phi =$
  $$\boldsymbol{e}_r \left(\frac{R^3}{r^3} - 1\right) \boldsymbol{u}\cdot\boldsymbol{e}_r - \boldsymbol{e}_\theta \left(\frac{R^3}{2r^3} + 1\right) \boldsymbol{u}\cdot\boldsymbol{e}_\theta = -\boldsymbol{u} + \frac{R^3}{2r^3}\, [3\boldsymbol{e}_r(\boldsymbol{u}\cdot\boldsymbol{e}_r) - \boldsymbol{u}],$$
  using $\boldsymbol{u} = \boldsymbol{e}_r(\boldsymbol{u}\cdot\boldsymbol{e}_r) + \boldsymbol{e}_\theta(\boldsymbol{u}\cdot\boldsymbol{e}_\theta) = \boldsymbol{e}_r u\cos\theta - \boldsymbol{e}_\theta u \sin\theta$ in the last step

CITA–ICAT

Potential flow around a sphere vs. AMR simulation

v_x, v_y, v_z in the plane of the initial B-field

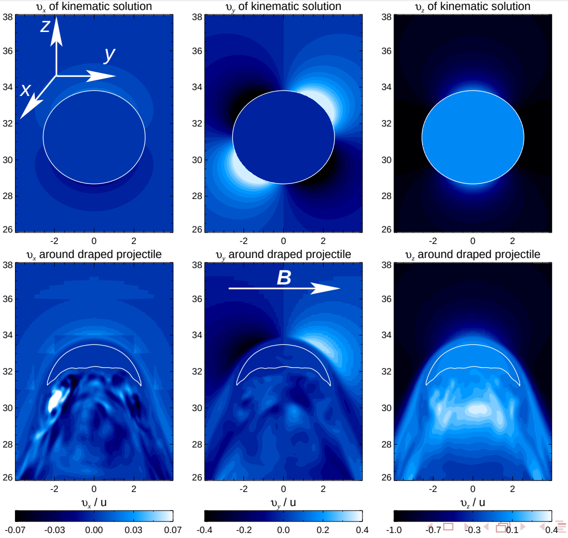

CITA–ICAT

Exact MHD solution: kinetic approximation

$$\mathrm{curl}(\boldsymbol{v} \times \boldsymbol{B}) = \boldsymbol{0} \qquad \mathrm{div}\boldsymbol{B} = 0$$

- given our potential flow solution for the velocity field, we can solve for the magnetic field $\boldsymbol{B}$
- homogeneous magnetic field at $z = \infty$
- this yields four coupled, linear, homogeneous, first order partial differential equations which can be solved by the method of characteristics

CITA–ICAT

Exact MHD solution: kinetic approximation

$$\mathrm{curl}(\boldsymbol{v} \times \boldsymbol{B}) = \boldsymbol{0} \qquad \mathrm{div}\boldsymbol{B} = 0$$

$$B_r = \frac{r^3 - R^3}{r^3} \cos\theta \left[C_1 \mp B_0 \sin\phi \int_\xi^r \frac{p(r,\theta) r'^4 \, \mathrm{d}r'}{(r'^3 - R^3 - p(r,\theta)^2 r')^{3/2} \sqrt{r'^3 - R^3}} \right],$$

$$B_\theta = \frac{2r^3 + R^3}{r^{5/2}\sqrt{r^3 - R^3}} \left[C_2 \pm 2 B_0 \sin\phi \int_\xi^r \frac{r'^3 (r'^3 + 2R^3)\sqrt{r'^3 - R^3} \, \mathrm{d}r'}{(2r'^3 + R^3)^2 \sqrt{r'^3 - R^3 - p(r,\theta)^2 r'}} \right],$$

$$B_\phi = \frac{B_0 \cos\phi}{\sqrt{1 - R^3/r^3}}, \qquad p(r,\theta) = r \sin\theta \sqrt{1 - \frac{R^3}{r^3}},$$

where C_1 and C_2 are integration constants, ξ is the initial value for which B_r and B_θ are known, upper signs refer to the upper half-space and vice versa.

CITA–ICAT

Approximate MHD solution near the sphere

$$\mathrm{curl}(\boldsymbol{v} \times \boldsymbol{B}) = \boldsymbol{0} \qquad \mathrm{div}\boldsymbol{B} = 0$$

$$\begin{aligned} B_r &= \frac{2}{3} B_0 \sqrt{\frac{3s}{R}} \frac{\sin\theta}{1+\cos\theta} \sin\phi, \\ B_\theta &= B_0 \sin\phi \sqrt{\frac{R}{3s}}, \\ B_\phi &= B_0 \cos\phi \sqrt{\frac{R}{3s}}, \end{aligned}$$

where $s = r - R$. These equations uniformly describe the field near the sphere with respect to the angle θ.

CITA–ICAT

MHD solution: kinematic approx. vs. AMR simulation

B_x, B_y, B_z in the plane of the initial B-field

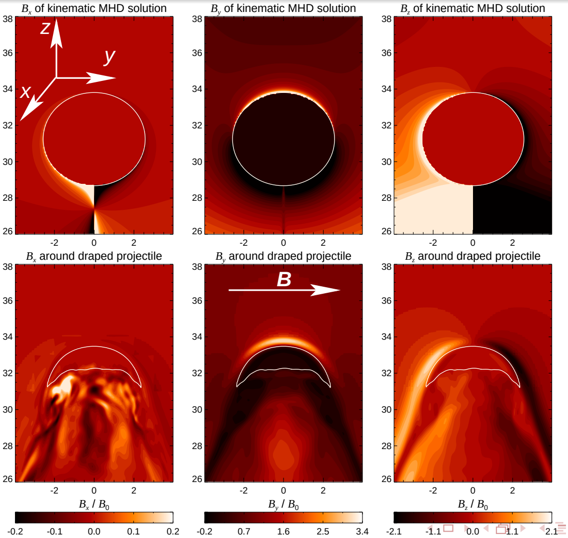

CITA–ICAT

MHD solution: kinematic approx. vs. AMR simulation

B_x, B_y, B_z in the plane perpendicular to the initial B-field

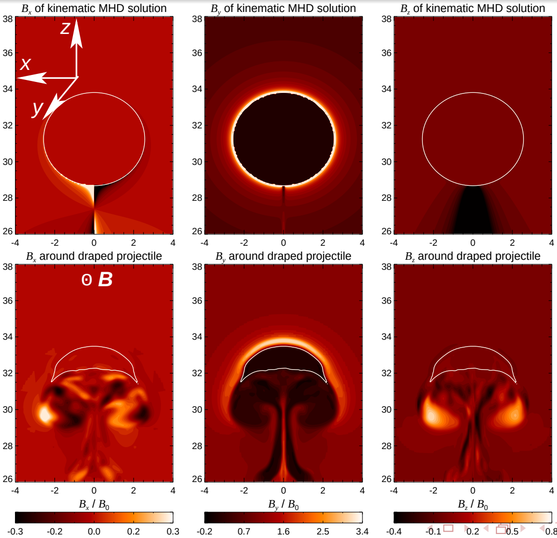

CITA–ICAT

Thickness of the draping sheath - analytics

Energy density of magnetic draping sheath balances ram pressure:

$$\begin{aligned} B &= \frac{B_0}{\sqrt{1-\frac{R^3}{(R+s)^3}}} \approx \sqrt{\frac{R}{3s}}B_0 + \mathcal{O}\left(\sqrt{\frac{s}{R}}\right) \\ P_B &= \frac{B^2}{8\pi} = P_{B_0}\frac{R}{3s} = \alpha\rho_0 u^2 \\ \mathcal{M}_\mathrm{A}^2 &= \frac{\rho_0 u^2}{2P_{B_0}} = \frac{1}{2}\beta\gamma\mathcal{M}^2 \\ l_\mathrm{drape} &\equiv s = \frac{R}{6\alpha\mathcal{M}_\mathrm{A}^2} = \frac{R}{3\alpha\beta\gamma\mathcal{M}^2} \sim 100\,\mathrm{pc}, \end{aligned}$$

for $R \simeq 30$ kpc, $\beta = P_\mathrm{th}/P_B \simeq 50$, and a trans-sonic flow, $\mathcal{M}^2 \simeq 1/\gamma$.

Thickness of the draping sheath – simulations

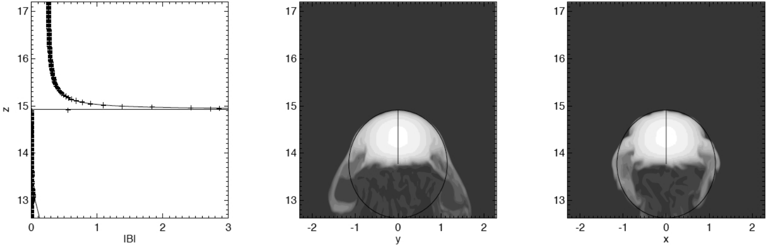

amplified draping field $B = \frac{1}{\sqrt{1-\frac{R^3}{r^3}}} B_0$, $l_{\mathrm{drape}} \simeq \frac{R}{6\alpha\mathcal{M}_{\mathrm{A}}^2}$ with $\alpha \simeq 2$;

left: fitting peak position and a fall-off radius of the theory prediction; *right:* density cut-planes; circle shows radius and position given by the fit to the magnetic field structure, left;

→ astonishing agreement of curvature radius at the working surface with potential flow predictions!

CITA–ICAT

Why caring about an analytical solution?

- obtain correct scaling of draping thickness, condition on λ_B, etc. with dimensionless parameters in the problem, $\mathcal{M}_\mathrm{A}, \ldots$
- calculating constraints on physical parameters that we can afford given our resolution constraints $l_\mathrm{drape} \gtrsim \Delta x$ and $R = L\sqrt{2}/4$:

$$l_\mathrm{drape} \equiv s = \frac{R}{6\alpha\mathcal{M}_\mathrm{A}^2} = \frac{R}{3\alpha\beta\gamma\mathcal{M}^2} \sim 100\,\mathrm{pc},$$

$$\beta_\mathrm{sim} \lesssim \frac{\sqrt{2}N}{12\alpha\gamma\mathcal{M}^2} \simeq 50\ (100) \quad \text{for } N = 768\ (1280)$$

CITA–ICAT

Outline

CITA–ICAT

Polarized synchrotron emission in a field spiral: M51

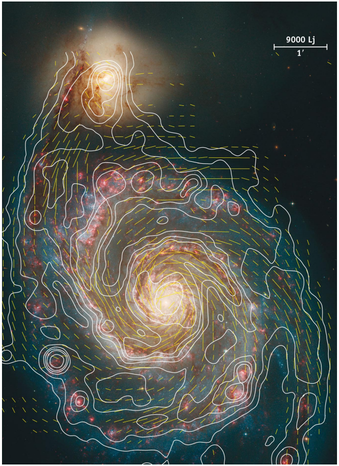

MPIfR Bonn and Hubble Heritage Team

- polarized synchrotron intensity follows the spiral pattern and is strongest in between the spiral arms
- the polarization 'B-vectors' are aligned with the spiral structure
- a promising generating mechanism is the *dynamo which transfers mechanical into magnetic energy* (Beck et al. 1996)
- efficient dynamo needs turbulent motions and non-uniform (differential) rotation of the disk

CITA–ICAT

Ram-pressure stripping of cluster spirals

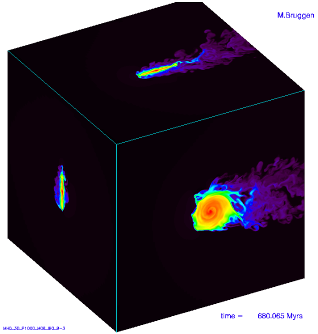

Brueggen (JU Bremen)

- 3D hydrodynamical simulations show that low-density gas in between spiral arms is quickly stripped irrespective of disk radius (Tonnesen & Bryan 2010)
- being flux-frozen into this dilute plasma, the large scale field will also be stripped, leaving behind the small scale field in the star forming regions

→ beam depolarization effects and superposition of causally unconnected star forming patches along the line-of-sight cause the resulting radio synchrotron emission to be effectively unpolarized

CITA–ICAT

Polarized synchrotron ridges in Virgo spirals

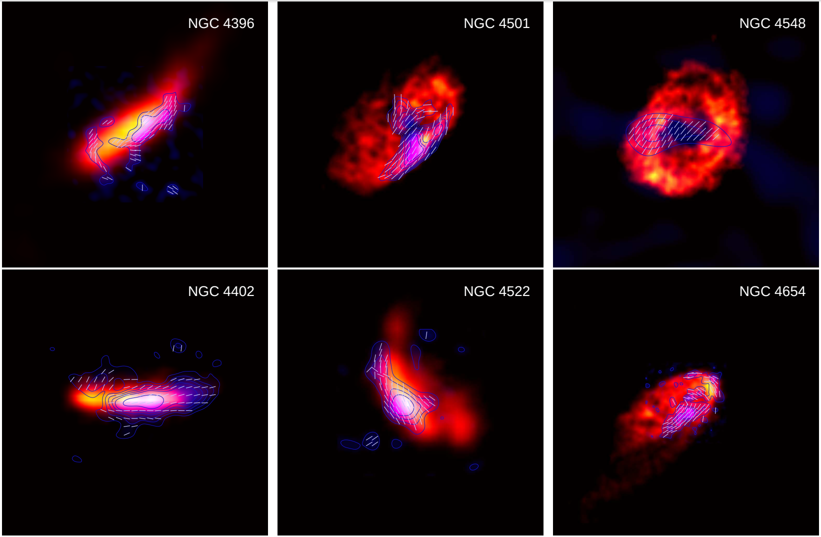

Vollmer et al. (2007): 6 cm PI (contours) + B-vectors; Chung et al. (2009): HI (red)

Observational evidence and model challenges

- asymmetric distributions of polarized intensity at the leading edge with extraplanar emission, sometimes also at the side
- coherent alignment of polarization vectors over $\sim$ 30 kpc
- stars lead polarized emission, polarized emission leads gas
- HI gas only moderately enhanced (factor $\lesssim 2$), localized 'HI hot spot' smaller than the polarized emission region: $n_\mathrm{compr} \simeq n_\mathrm{icm}\, \upsilon_\mathrm{gal}^2 / c_\mathrm{ism}^2 \simeq 1\,\mathrm{cm}^{-3} \simeq \langle n_\mathrm{ism} \rangle$
- flat radio spectral index (similar to the Milky Way) that steepens towards the edges of the polarized ridge
- no or weak Kelvin-Helmholtz instabilities at interface detectable

$\rightarrow$ previous models that use ram-pressure compressed galactic magnetic fields fail to explain most of these points!

CITA–ICAT

Observational evidence and model challenges

- asymmetric distributions of polarized intensity at the leading edge with extraplanar emission, sometimes also at the side
- coherent alignment of polarization vectors over $\sim$ 30 kpc
- stars lead polarized emission, polarized emission leads gas
- HI gas only moderately enhanced (factor $\lesssim 2$), localized ‘HI hot spot’ smaller than the polarized emission region:
  $n_\text{compr} \simeq n_\text{icm}\, \upsilon_\text{gal}^2 / c_\text{ism}^2 \simeq 1\,\text{cm}^{-3} \simeq \langle n_\text{ism} \rangle$
- flat radio spectral index (similar to the Milky Way) that steepens towards the edges of the polarized ridge
- no or weak Kelvin-Helmholtz instabilities at interface detectable

$\rightarrow$ need to consider the full MHD of the interaction spiral galaxy and magnetized ICM !

Magnetic draping around a spiral galaxy – MHD

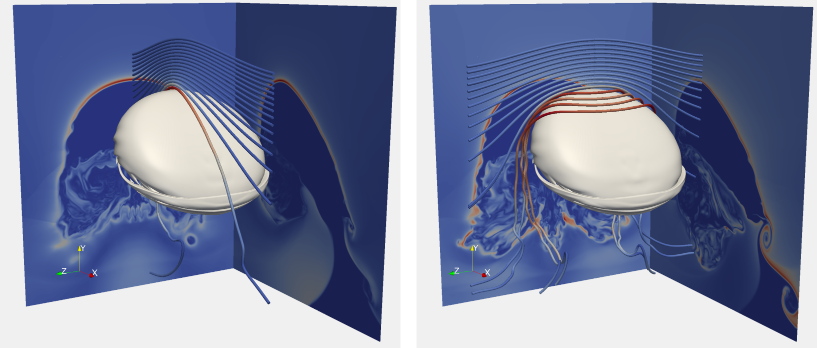

Athena simulations of spiral galaxies interacting with a uniform cluster magnetic field. There is a sheath of strong field draped around the leading edge (field strength is color coded).

CITA–ICAT

Magnetic draping around a spiral galaxy – physics

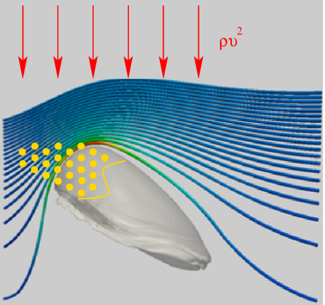

- the galactic ISM is pushed back by the ram pressure wind $\sim \rho \upsilon^2$
- the stars are largely unaffected and lead the gas
- the draping sheath is formed at the contact of ISM/ICM
- as stars become SN, their remnants accelerate CRes that populate the field lines in the draping layer
- CRes are transported diffusively (along field lines) and advectively as field lines slip over the galaxy
- CRes emit radio synchrotron radiation in the draped region, tracing out the field lines there $\rightarrow$ coherent polarized emission at the galaxies' leading edges

CITA–ICAT

Modeling the electron population

- cooling time scale of synchrotron emitting electrons (CRe):

$$\nu_{\rm sync} = \frac{3eB}{2\pi\, m_{\rm e} c}\gamma^2 \simeq 5\ {\rm GHz} \left(\frac{B}{7\,\mu{\rm G}}\right)\left(\frac{\gamma}{10^4}\right)^2,$$

$$\tau_{\rm sync} = \frac{E}{\dot{E}} = \frac{6\pi m_{\rm e} c}{\sigma_{\rm T} B^2 \gamma} = 5\times 10^7\ {\rm yr}\left(\frac{\gamma}{10^4}\right)^{-1}\left(\frac{B}{7\,\mu{\rm G}}\right)^{-2}$$

- typical SN rates imply a homogeneous CRe distribution (WMAP)
- FIR-radio correlation of Virgo spirals show comparable values to the solar circle: take MW CRe distribution inside our galaxies,

$$n_{\rm cre} = C_0\, e^{-(R-R_\odot)/h_R}\, e^{-|z|/h_z}$$

  with normalization $C_0 \simeq 10^{-4}\,{\rm cm}^{-3}$ as well as scale heights $h_R \simeq 8\,{\rm kpc}$ and $h_z \simeq 1\,{\rm kpc}$, normalized at Solar position
- truncate at contact of ISM-ICM, attach exp. CRe distribution $\perp$ to contact surface with $h_\perp \simeq 150$ pc (max. radius of Sedov phase)

CITA–ICAT

Magnetic draping and polarized synchrotron emission

Synchrotron B-vectors reflect the upstream orientation of cluster magnetic fields

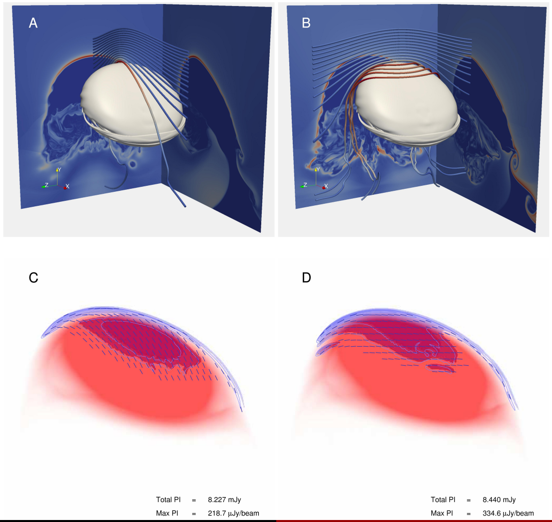

CITA–ICAT

Simulated polarized synchrotron emission

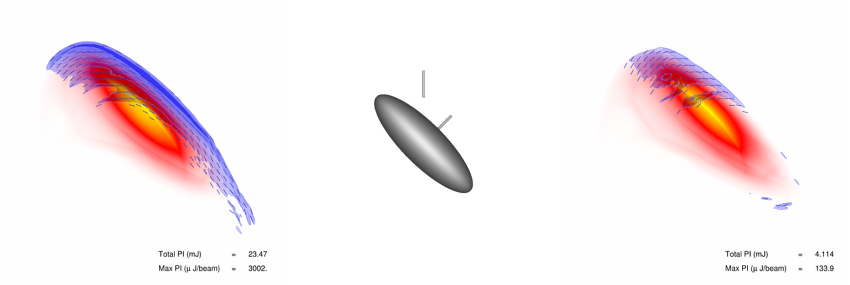

Movie of the simulated polarized synchrotron radiation viewed from various angles and with two field orientations.

Streamlines in the rest frame of the galaxy

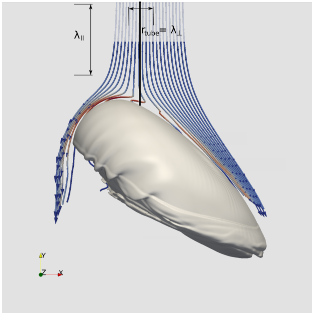

- as the flow approaches the galaxy it decelerates and gets deflected
- only those streamlines initially in a narrow tube of radius $\lambda_{\perp} \simeq R/\sqrt{3\beta\mathcal{M}^2} \simeq R/15 \simeq 1.3$ kpc from the stagnation line become part of the magnetic draping layer (color coded) $\rightarrow$ constraints on λ_B
- the streamlines that do not intersect the tube get deflected away from the galaxy, become never part of the drape and eventually get accelerated (Bernoulli effect)
- note the kink feature in some draping-layer field lines due to back reaction as the solution changes from the hydrodynamic potential flow solution to that in the draped layer

CITA–ICAT

Magnetic draping of a helical B-field

(Non-)observation of polarization twist constrains magnetic coherence length

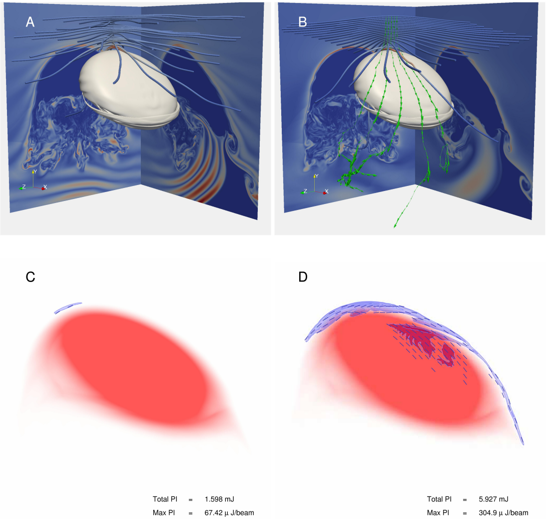

CITA–ICAT

Magnetic coherence scale estimate by radio ridges

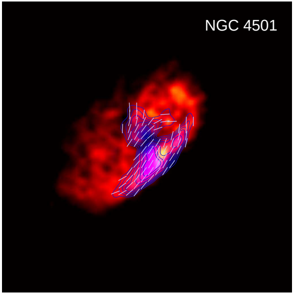

- observed polarised draping emission $\rightarrow$ field coherence length λ_B is at least galaxy-sized
- if $\lambda_B \sim 2R_{\rm gal}$, then the change of orientation of field vectors imprint as a change of the polarisation vectors along the vertical direction of the ridge showing a ‘polarisation-twist’
- the reduced speed of the boundary flow means that a small $L_{\rm drape}$ corresponds to a larger length scale of the unperturbed magnetic field ahead of the galaxy NGC 4501

$$L_{\rm coh} \simeq \eta L_{\rm drape} v_{\rm gal}/v_{\rm drape} = \eta \tau_{\rm syn} v_{\rm gal} > 100\,{\rm kpc},$$

with $\tau_{\rm syn} \simeq 5 \times 10^7$ yr, $v_{\rm gal} \simeq 1000\,{\rm km/s}$, and a geometric factor $\eta \simeq 2$

Varying galaxy inclination and magnetic tilt

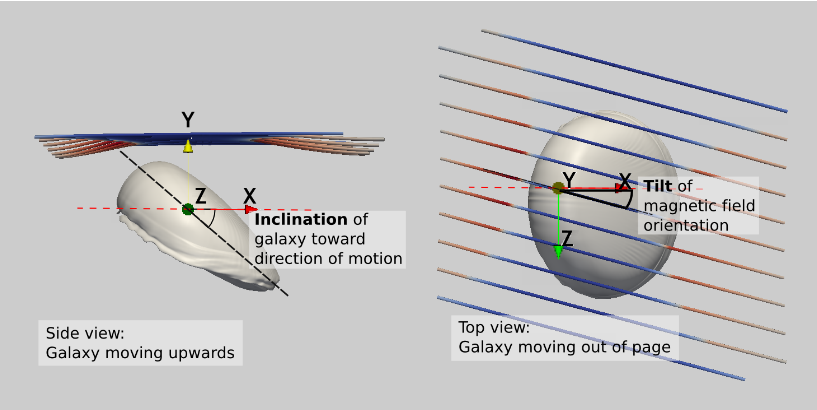

CITA–ICAT

Observations versus simulations

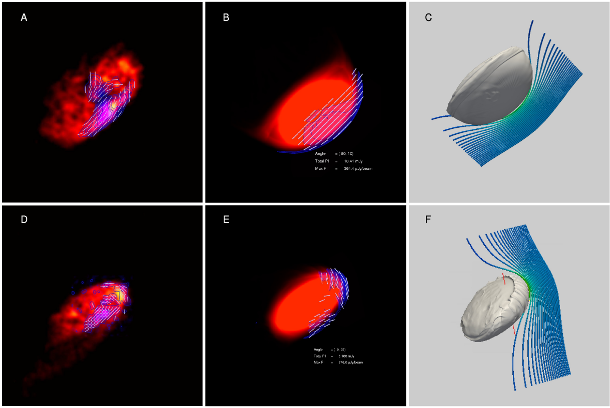

HI emission of two spirals (red) is compared to the polarized radio synchrotron ridges at 6 cm (blue and contours) and B-vectors.

CITA–ICAT

Biases in inferring the field orientation

- uncertainties in estimating the 3D velocity: v_r, ram-pressure stripped gas visible in HI morphology $\rightarrow \hat{\boldsymbol{v}}_\mathrm{t}$
- *direction-of-motion asymmetry:* magnetic field components in the direction of motion bias the location of $B_\text{max, drape}$ (figure to the right): draping is absent if $\boldsymbol{B} \parallel \boldsymbol{v}_\mathrm{gal}$

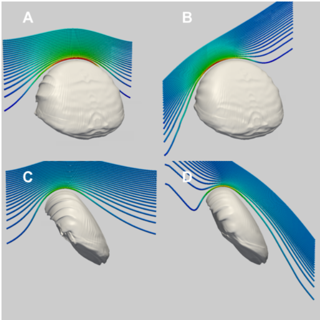

- *geometric bias:* polarized synchrotron emission only sensitive to traverse magnetic field B_t ($\perp$ to LOS) $\rightarrow$ maximum polarised intensity may bias the location of $B_\text{max, drape}$ towards the location in the drape with large B_t

Outline

1. Magnetic draping
   - Space physics and clusters
   - Analytical calculations
   - MHD Simulations
2. Spiral galaxies
   - Polarized radio ridges
   - Physics of magnetic draping
   - Draping and synchrotron emission
3. Implications
   - Magnetic field orientations
   - Kinetic plasma instabilities
   - Cosmological evolution of galaxy clusters

Mapping out the magnetic field in Virgo

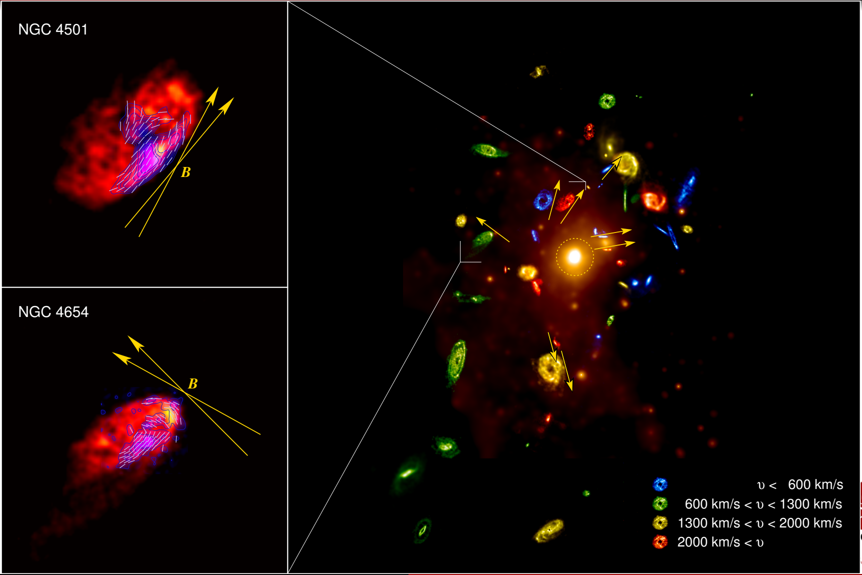

Discussion of radial field geometry

- The alignment of the field in the plane of the sky is significantly more radial than expected from random chance. Considering the sum of deviations from radial alignment gives a chance coincidence of less than 1.7% ($\sim 2.2\,\sigma$).[1]
- For the three nearby galaxy pairs in the data set, all have very similar field orientations.
- The isotropic distribution with respect to the centre (M87) is difficult to explain with the past activity of the central AGN.

$\rightarrow$ Which effect causes this field geometry?

[1] Caveat: this statistical analysis does not include systematic uncertainties such as line-of-sight effects.

CITA–ICAT

Magneto-thermal instability: the idea

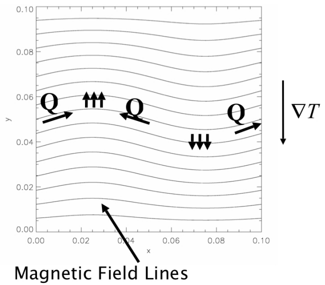

Figure from I. Parrish

Convective stability in a gravitational field:

- Classical Schwarzschild criterion: $\frac{dS}{dz} > 0$
- long MFP, Balbus criterion: $\frac{dT}{dz} > 0$
- new instability causes field lines to reorient radially → efficient thermal conduction radially (close to Spitzer)

The non-linear behavior of the MTI (Parrish & Stone 2007).

- Adiabatic boundary conditions for $T(r)$: the instability can exhaust the source of free energy → isothermal profile
- Fixed boundary conditions for $T(r)$: field lines stay preferentially radially aligned (35 deg mean deviation from radial)

CITA–ICAT

Magneto-thermal instability: the idea

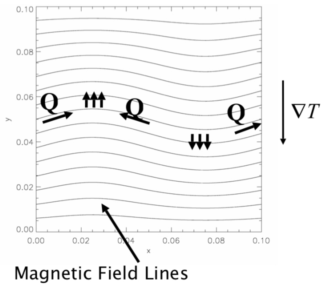

Figure from I. Parrish

Convective stability in a gravitational field:

- Classical Schwarzschild criterion: $\frac{\mathrm{d}S}{\mathrm{d}z} > 0$
- long MFP, Balbus criterion: $\frac{\mathrm{d}T}{\mathrm{d}z} > 0$
- new instability causes field lines to reorient radially $\rightarrow$ efficient thermal conduction radially (close to Spitzer)

The non-linear behavior of the MTI (Parrish & Stone 2007).

- Adiabatic boundary conditions for $T(r)$: the instability can exhaust the source of free energy $\rightarrow$ isothermal profile
- Fixed boundary conditions for $T(r)$: field lines stay preferentially radially aligned (35 deg mean deviation from radial)

CITA–ICAT

Gravitational shock wave heating

The observed temperature profile in clusters is decreasing outwards which is the necessary condition for MTI to operate → *gravitational heating can stabilize the temperature profile:*

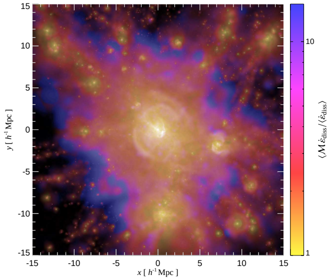

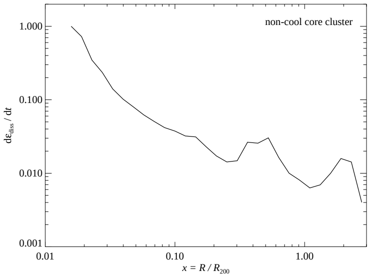

Mach number distribution weighted by $\varepsilon_{\rm diss}$.

Energy flux through shock surface $\dot{E}_{\rm diss}/R^2 \sim \rho\upsilon^3 \rightarrow$ increase towards the center

CITA–ICAT

Implications for thermal stability of galaxy clusters

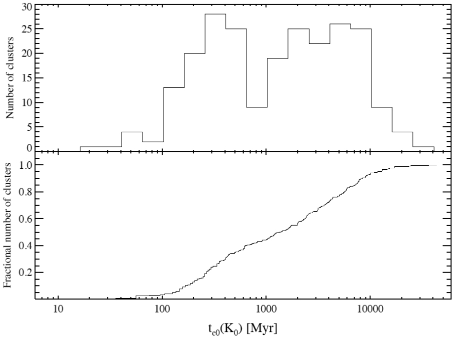

Cavagnolo et al. (2009)

- radial fields in non-cool core clusters (NCCs) imply efficient thermal conduction that stabilizes these systems against entering a cool-core state: $\tau_{\text{cond}} = \lambda^2/\chi_C \simeq 2.3 \times 10^7\,\text{yr}\,(\lambda/100\,\text{kpc})^2$, where χ_C is the Spitzer thermal diffusivity (using $kT = 10\,\text{keV}$, $n = 5 \times 10^{-3}\,\text{cm}^{-3}$)
- current cosmological cluster simulations fail to reproduce NCCs that have no AGN activity $\rightarrow$ MHD + anisotropic conduction

CITA–ICAT

Speculation: evolutionary sequence of galaxy clusters

- After a merging event of a non-cool core cluster, the injected turbulence decays on an eddy turnover time $\tau_{\rm eddy} \simeq L_{\rm eddy}/\upsilon_{\rm turb} \sim 300\,\mathrm{kpc}/(300\,\mathrm{km/s}) \sim 1$ Gyr.
- The magneto-thermal instability grows on a similar timescale of less than 1 Gyr and the magnetic field becomes radially oriented.
- The efficient thermal conduction stabilizes this cluster until a cooling instability in the center may cause the cluster to enter a cooling core state – similar to Virgo now – and requires possibly feedback by an active galactic nuclei to be stabilized.

CITA–ICAT

Conclusions on magnetic draping around galaxies

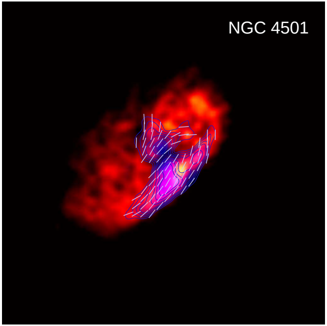

- draping of cluster magnetic fields naturally explains polarization ridges at Virgo spirals

Conclusions on magnetic draping around galaxies

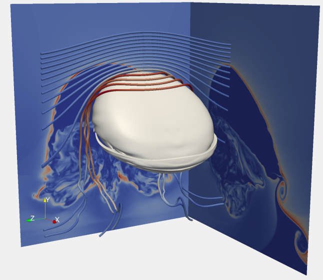

- draping of cluster magnetic fields naturally explains polarization ridges at Virgo spirals
- this represents a new tool for measuring the in situ 3D orientation and coherence scale of cluster magnetic fields

CITA–ICAT

Conclusions on magnetic draping around galaxies

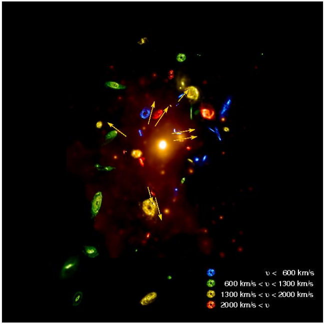

- draping of cluster magnetic fields naturally explains polarization ridges at Virgo spirals
- this represents a new tool for measuring the in situ 3D orientation and coherence scale of cluster magnetic fields
- application to the Virgo cluster shows that the magnetic field is preferentially aligned radially

CITA–ICAT

Conclusions on magnetic draping around galaxies

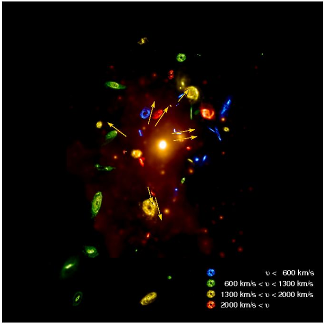

- draping of cluster magnetic fields naturally explains polarization ridges at Virgo spirals
- this represents a new tool for measuring the in situ 3D orientation and coherence scale of cluster magnetic fields
- application to the Virgo cluster shows that the magnetic field is preferentially aligned radially

- this finding is suggestive that the MTI may be operating and implies efficient thermal conduction close to the Spitzer value
- it also proposes that non-cool core clusters are stabilized by thermal conduction

CITA–ICAT

Literature for the talk

- Pfrommer & Dursi, 2010, Nature Phys., published online, arXiv:0911.2476, *Detecting the orientation of magnetic fields in galaxy clusters*
- Dursi & Pfrommer, 2008, ApJ, 677, 993, *Draping of cluster magnetic fields over bullets and bubbles - morphology and dynamic effects*